Near field distributions of resonant modes in small dielectric objects on flat surfaces

J. R. Arias-González and M. Nieto-Vesperinas *

Instituto de Ciencia de Materiales de Madrid, Consejo Superior de Investigaciones Científicas, Campus de Cantoblanco, 28049 Madrid. Spain.

Abstract

We report numerical simulations on the coupling of waves, either propagating or evanescent, with the eigenmodes of dielectric nanocylinders and nanospheres on substrates. The multiple interaction of light between these objects and the dielectric surface at which the evanescent waves are created, is taken into account. In this way, we present an accurate procedure to predict and control the creation of large field enhancements concentrated both within and near the nanoparticle, versus the angle of incidence and the state of polarization.

Recently, much interest has arosed on the excitation of electromagnetic eigenmodes of small particles (both plasmon for metallic large particles [1] and Mie resonances for dielectric ones [2–6]). This stems from their use in field concentration for near field optical studies and as high-Q cavity devices. The behavior of the near field strongly depends on the size and refractive index of the particles, as well as on the state of polarization and wavevector of the exciting wave. Therefore, it is desirable to put forward a method that can predict how the incident field (either propagating or evanescent) will excite the near field in the particle, and how the resonant field distribution corresponding to an eigenmode will build

*Corresponding author's e-mail address, mnieto@icmm.csic.es

up. This is the purpose of this letter. We place the particle in the proximity of a dielectric surface so that the theory must exactly account for the wave multiple interaction between both bodies, whether or not with existence of total internal reflection (TIR) at the surface.

The calculation will mainly be concentrated on cylinders in a 2-D configuration, however, we shall also compare with results for spheres in 3-D. We shall also discuss how the presence of the dielectric surface affects the field distribution that would appear in the situation of an isolated particle. The surface here considered is flat, but the method equally yields accurate results when it is corrugated.

The exact numerical calculations are based on the integral method previously reported [7]. These show remarkable high near field enhancements due to Mie resonance excitations within small particles with size parameter $x = 2\pi a/\lambda \lesssim 1$ (a being the radius of the particle). Silicon particles have been simulated [8], yielding high field concentrations. Near field enhancements had previously been found for larger particles ($x \gg 1$) [9–11].

Resonant excitation is produced with incident waves transmitted at the flat interface separating glass ($n = 1.52$) from air, where the small particle is placed at distance d (see the inset of Fig. 1(b)). The angle of incidence θ_0 is set to either zero (normal incidence) or $\theta_0 = 60^o$, where TIR in the absence of particle occurs (the critical angle is $\theta_c = 41.14^o$). We use Gaussian incident beams of half width at half maximum (HWHM) W large enough to also resemble results from an incident plane wave. For reference, some calculations for the isolated particle are presented. These are Mie's when the incident wave is propagating, and derived from our method when it is evanescent.

Figs. 1 show the scattering efficiencies for an isolated particle in vacuum with size either $a = 60$ nm or $a = 200$ nm. We compare results from a full 3-D situation of a sphere (Fig. 1(a)) with a 2-D configuration, namely, a cylinder with its axis normal to the incidence plane (Figs. 1(b), (c) and (d)). The incident field is either propagating or evanescent, created with $\theta_o = 60^o$, S-polarized (electric field parallel to the cylinder axis) or P-polarized (magnetic field parallel to the cylinder axis). When the incident wave is evanescent, the intensity is normalized to the incident intensity averaged over the cross-sectional area of the sample

perpendicular to the incident Poynting vector. Namely, to:

$$\tilde{\mathrm{I}}_0 = \frac{1}{2a}\int \langle \mathbf{S_{inc}} \rangle \, \mathbf{n} dA = I_0 \frac{n_0}{n_1} \sin\theta_0 \exp(-2\kappa d) \frac{\sinh(2\kappa a)}{2\kappa a} \tag{1}$$

where n_0 and n_1 are the refractive indices of air and the particle, respectively, $\kappa = 2\pi/\lambda(n_0^2 \sin^2\theta_0 - n_1^2)^{1/2}$ and I_0 represents the incident intensity. This kind of normalization has been previously reported [12]. These far field calculations show that results obtained for cylinders are similar to those obtained for spheres. We have also checked that the peak positions and half widths of the scattering efficiency are unaffected by the kind of excitation (i.e., either propagating or evanescent). However, the peak height depends on this excitation, being larger for evanescent waves. This efficiency difference is more important as the size of the cylinder increases.

Fig. 2 shows the normalized near field intensity spatial distribution ($|H/H_o|^2$, H_o being the incident magnetic field) for a silicon cylinder with radius $a = 60$ nm on the dielectric plane at distance $d = 5$ nm for P polarization at the resonant wavelengths (cf. Fig. 1(c)): $\lambda = 471$ nm $[n = (4.485, 0.101)]$, Figs. 2(a) and 2(c), and $\lambda = 638$ nm $[n = (3.872, 0.018)]$, Figs. 2(b) and 2(d) respectively. The length of the plane dielectric surface in the computation is $L = 34000$ nm, $W = 4000$ nm. Large field concentrations are obtained for P polarization. However, for S polarization the field distribution spreads outside the cylinder with a no so high enhancement inside (not shown here for the sake of brevity). This behavior of the near field distribution remains at both wavelengths: P polarization concentrates almost all the incident field inside the cylinder leading to low eigenmodes. On the other hand, evanescent incident wave excitation (created under TIR) shifts this distribution to that of the coupling with the surface wave refracted under TIR, i.e. it rotates this near field intensity distribution by 90^o, and slightly displaces it towards the flat surface. Notice that the lower values of this intensity are due to the decay of the evanescent wave at the cylinder. At the same time, evanescent wave excitation is more effective for field concentration, since the ratio of the intensity field distribution to that of the incident intensity along the plane $z = d + a$, is larger in this case. For such small cylinder sizes, multiple scattering effects

between the flat surface and the cylinder are not very large. These effects generally broaden, damp and slightly red-shift the resonance lineshapes [7].

Fig. 3 shows calculations for a larger cylinder (radius $a = 200$ nm) at distance $d = 15$ nm from the surface. Again $W = 4000$ nm at the resonant wavelength $\lambda = 760$ nm, $\theta_o = 0^o$ (Fig. 3(a)) and $\lambda = 761$ nm, $\theta_o = 60^o$ (Fig. 3(b)) (cf. Fig. 1(d)), $n = (3.728, 0.009)$. This resonance is red-shifted by 1 nm by the presence of the flat surface for plane wave excitation (i.e. from 759 to 760 nm) and by 2 nm for evanescent wave excitation (namely from 759 to 761 nm). The corresponding near field distribution intensity falls about 60% for an incident plane wave and by 44% for an incident evanescent wave with respect to the case of an isolated cylinder (i.e. with no surface present). On the other hand, this cylinder size ($a = 200$ nm) presents a greater enhancement than the previous situation ($a = 60$ nm). In case of plane wave excitation (Fig. 3(a)) we see a lobe pattern that can be explained as a standing wave resulting from an interference phenomenom due to evanescent waves circumnavegating on the cylinder surface in opposite senses from bottom to top. In case of evanescent wave excitation (TIR incidence) only one propagation sense is allowed for the surface waves, showing in Fig. 3(b) a ring structure with a slight lobe pattern which has a lower contrast when no surface is present. This indicates that the conversion of evanescent waves on the plane into propagating waves by means of multiple scattering enhances the interference (see the inset in Fig 3(a)). We believe that for bigger sizes as the ones shown in Refs. [8–10], this effect is more noticeable as shown in previous works [2]. Again, the lobe structure formed under TIR illumination (Fig. 3(b)) is rotated, compared to that from plane wave excitation (Fig. 3(a)). This lobe pattern is related to the structure of multiple peaks shown in previous works (cf. Ref. [9]) near the surface with exponential decay outside larger cylinders, and it can also be attributed to resonant modes associated to internal waves traveling around the cylinder surface and undergoing internal reflections at the boundary. It is remarkable that these modes concentrate inside the volume of our small particles as a decreases, in contrast with their periferic distributions for larger particles as shown in Ref. [9]. The number of lobes must be $2n$ along the perimeter. The average field

intensity integrated on a circle, centered at the cylinder axis, as a function of the radius of the particle, must show l lobes. We have identifed through the corresponding Mie coefficient [9] that $n = 3$ and $l = 1$, for the resonance of Fig. 3. On the other hand, in Figs. 2(a) and 2(c) $n = 1$ and $l = 1$, and for Figs. 2(b) and 2(d) $n = 0$ and $l = 1$. The insets in Figs. 2(c), 2(d) and Fig. 3(b) show the amplitude of the external Mie coefficient for these resonances.

For comparison, Fig. 4 shows resonant near field distributions $|E/E_o|^2$ (E_o being the electric incident field) for propagating plane wave excitation on an isolated sphere with either $a = 60$ nm (Fig. 4(a)) or $a = 200$ nm (Fig. 4(b)). These are shown in a plane containing the sphere equator, parallel to the incident wavevector and perpendicular to the incident electric vector. We find Mie resonance distributions similar to those shown for a cylinder in Figs. 2 and 3, located at the wavelengths $\lambda = 521$ nm with $n = (4.195, 0.058)$, and $\lambda = 817$ nm with $n = (3.677, 0.005)$ (cf. Fig. 1(a)). However, these intensities are lower than for P polarization in a an isolated cylinder, since now the sphere produces both P and S polarized scattered waves, the amplitude of the latter spreading outside the particle, as explained above. The modes are identified [10] as TE with $n = 1$, $l = 1$ for $a = 60$ nm, and $n = 3$, $l = 1$ for $a = 200$ nm. The latter are rather similar to the whispering-gallery modes studied in larger particles (cf. Refs. [3–6]). It is worth remarking, however, that a study of the angular far field distributions has shown no privileged scattering angle of enhanced intensity, in contrast with glory backscattering effects that appear associated to certain Mie resonances in larger particles [13,14].

ACKNOWLEDGMENTS

Research supported by Fundación Ramón Areces and U.E. J.R. A-G. also thanks a scholarship from Comunidad Autónoma de Madrid.

REFERENCES

[1] J.R Krenn, A. Dereux, J.C. Weeber, E. Bourillot, Y. Lacroute, J.P. Goudonnet, G. Schider, W. Gotschy, A. Leitner, F.R. Aussenegg, and C. Girard, Phys. Rev. Lett. **82**, 2590-2593, (1999).

[2] C. Liu, T. Kaiser, S. Lange, G. Schweiger, Opt. Commun. **117**, 521-531 (1995).

[3] L. Collot, V. Lefèvre-Seguin, M. Brune, J.M. Raimond, and S. Haroche, Europhys. Lett. **23** (5), 327-334 (1993).

[4] J.C. Knight, N. Dubreuil, V. Sandoghdar, J. Hare, V. Lefèvre-Seguin, J.M. Raimond, and S. Haroche, Opt. Lett. **20** 1515-1517 (1995).

[5] D.S. Weiss, V. Sandoghdar, J. Hare, V. Lefèvre-Seguin, J.M. Raimond, and S. Haroche, Opt. Lett. **20**, 1835-1837, (1995).

[6] G. Griffel, S. Arnold, D. Taskent, A. Serpengüzel, J. Connolly, and N. Morris, Opt. Lett. **21**, 695-697, (1996).

[7] J.R. Arias-González, M. Nieto-Vesperinas, and A. Madrazo, J. Opt. Soc. Am. A **16**, 2928-2934 (1999).

[8] E.D. Palik (Ed.), *Handbook of Optical Properties of Solids*, Academic Press, London, 1985.

[9] J.F. Owen, R.K. Chang, and P.W. Barber, Opt. Lett. **6**, 540-542 (1981).

[10] P. Chylek, J.D. Pendleton, and R.G. Pinnick, Appl. Opt. **24**, 3940-3942 (1985).

[11] D.S. Benincasa, P.W. Barber, J-Z. Zhang, W-F. Hsieh, and R.K. Chang, Appl. Opt. **26**, 1348-1356 (1987).

[12] R. Wannemacher, A. Pack, and M. Quinten, Appl. Phys. B **68**, 225-232 (1999).

[13] H.C. Bryant and A.J. Cox, J. Opt. Soc. Am. **56**, 1529-1532 (1966).

[14] P.L. Marston and D.S. Langley, J. Opt. Soc. Am. **72**, 456-459 (1982).

FIGURE CAPTIONS

Figure 1: Scattering Efficiencies for: 1(a) Isolated sphere with radius either $a = 60$ nm (thick solid line) or $a = 200$ nm (thin solid line) excited by propagating plane wave. 1(c): Isolated cylinder with radius $a = 60$ nm excited by an incident wave as shown by the line code (either plane propagating or evanescent, created with $\theta_o = 60^o$). 1(b) and 1(d): Isolated cylinder with radius $a = 200$ nm excited by either an S or P polarized incident wave, respectively. The line code shows whether the incident wave is plane propagating or evanescent. The inset in 1(b) shows the scattering geometry.

Figure 2: Plots of $|H/H_o|^2$ for P polarization for a cylinder with $a = 60$ nm on a plane at $d = 5$ nm and $W = 4000$ nm. 2(a): $\lambda = 471$ nm, $\theta_o = 0^o$. 2(b): $\lambda = 638$ nm, $\theta_o = 0^o$. 2(c): $\lambda = 471$ nm, $\theta_o = 60^o$. 2(d): $\lambda = 638$ nm, $\theta_o = 60^o$. The circular lines show the boundary of the cylinder. Insets: real (solid line) and imaginary (dashed line) parts of the (n, l) external Mie coefficient amplitude.

Figure 3: Same as Fig. 2 for a cylinder with $a = 200$ nm at $d = 15$ nm. 3(a): $\lambda = 760$ nm, $\theta_o = 0^o$. 3(b): $\lambda = 761$ nm, $\theta_o = 60^o$ (TIR). Inset 3(a): normalized near field intensity along an internal circumference of radius $r = 125$ nm; solid and dashed thin lines: isolated cylinder excited by either a plane incident wave ($\theta_o = 0^o$) or a plane evanescent wave ($\theta_o = 60^o$), respectively. Solid and dashed thick lines: cylinder on a plane excited by a Gaussian incident beam of $W = 4000$ nm at either $\theta_o = 0^o$ or $\theta_o = 60^o$ (TIR), respectively. Inset 3(b): same as in Fig. 2.

Figure 4: Plots of $|E/E_o|^2$ for an isolated sphere illuminated by a plane incident wave, as shown by the picture inside 4(b). 4(a): $a = 60$ nm, $d = 5$ nm and $\lambda = 521$ nm. 4(b): $a = 200$ nm, $d = 15$ nm and $\lambda = 817$ nm. Insets: same as in Fig. 2 for the external Mie coefficient amplitude of the TE mode.

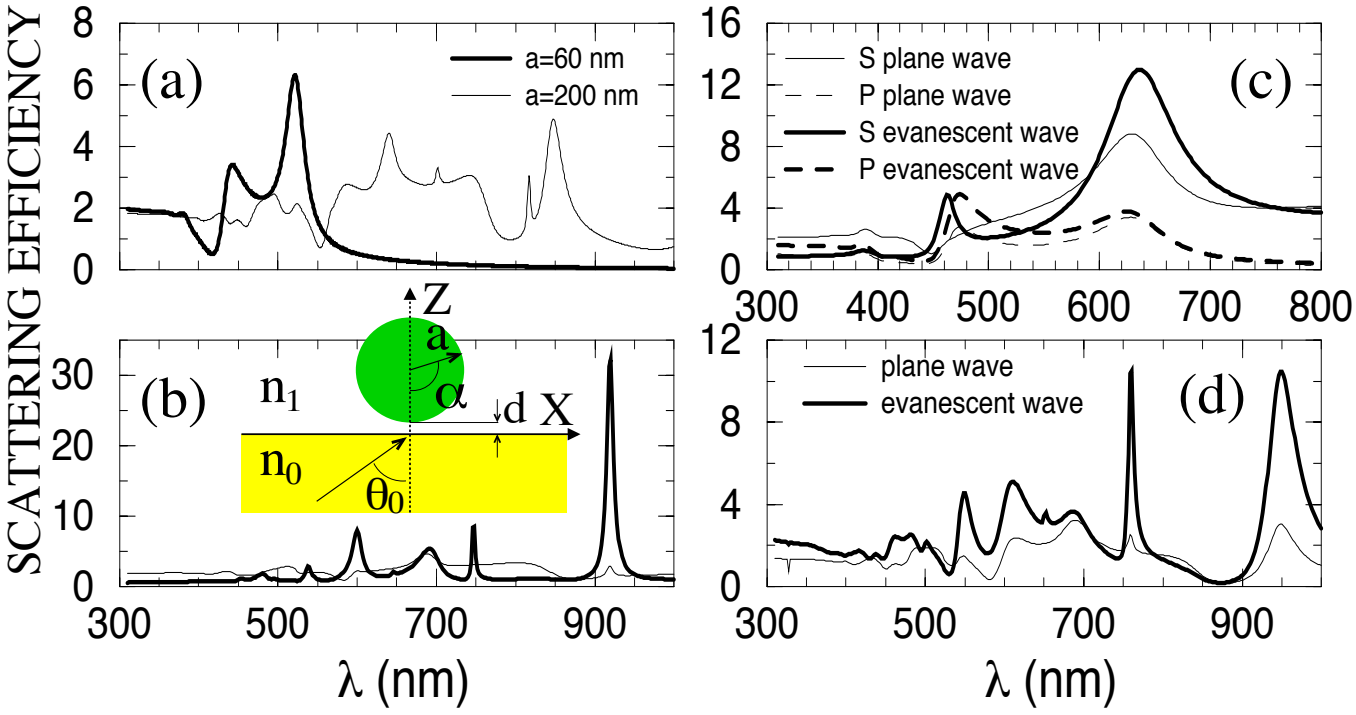

Fig. 1

J. R. Arias-Gonzalez et al.

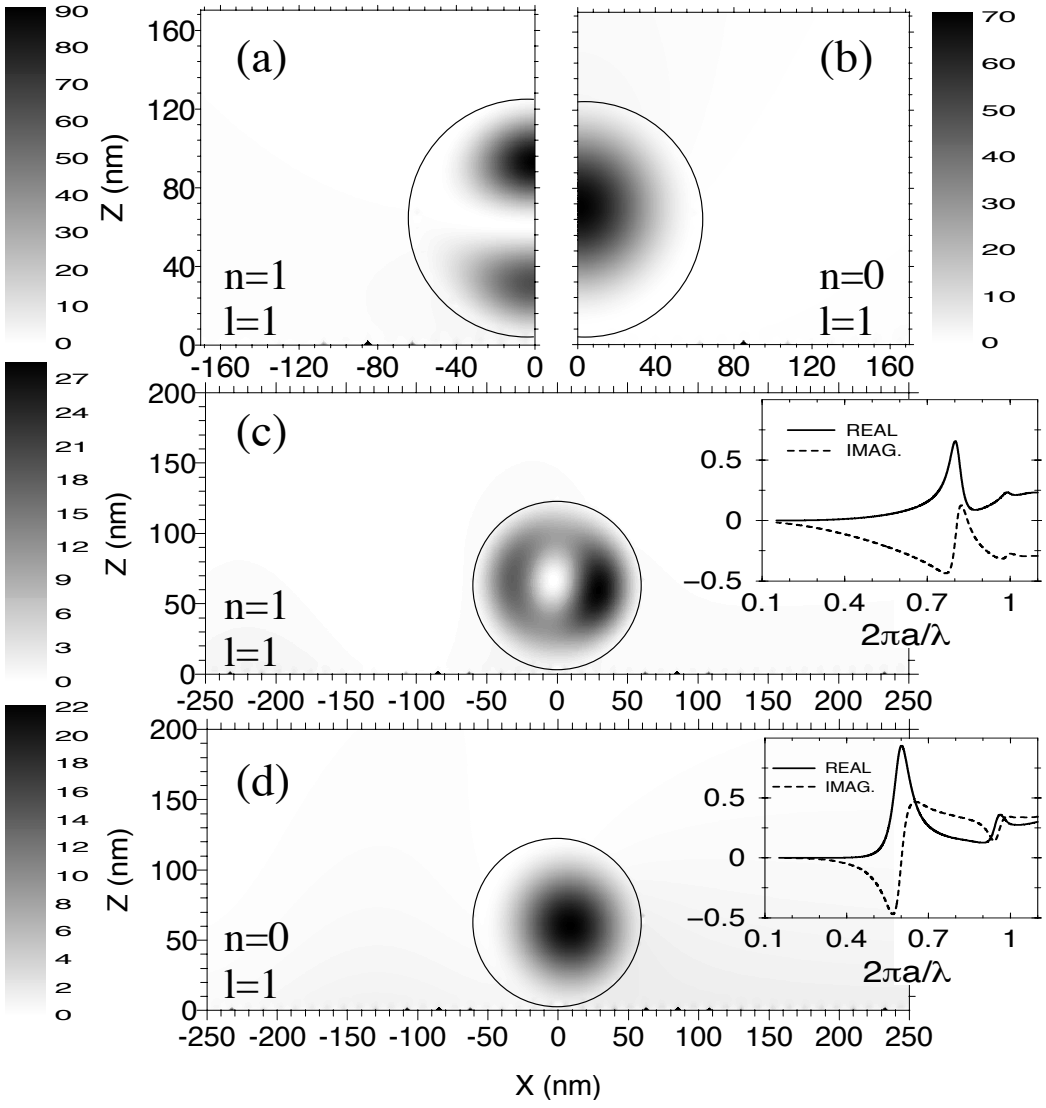

Fig. 2

J. R. Arias-Gonzalez et al.

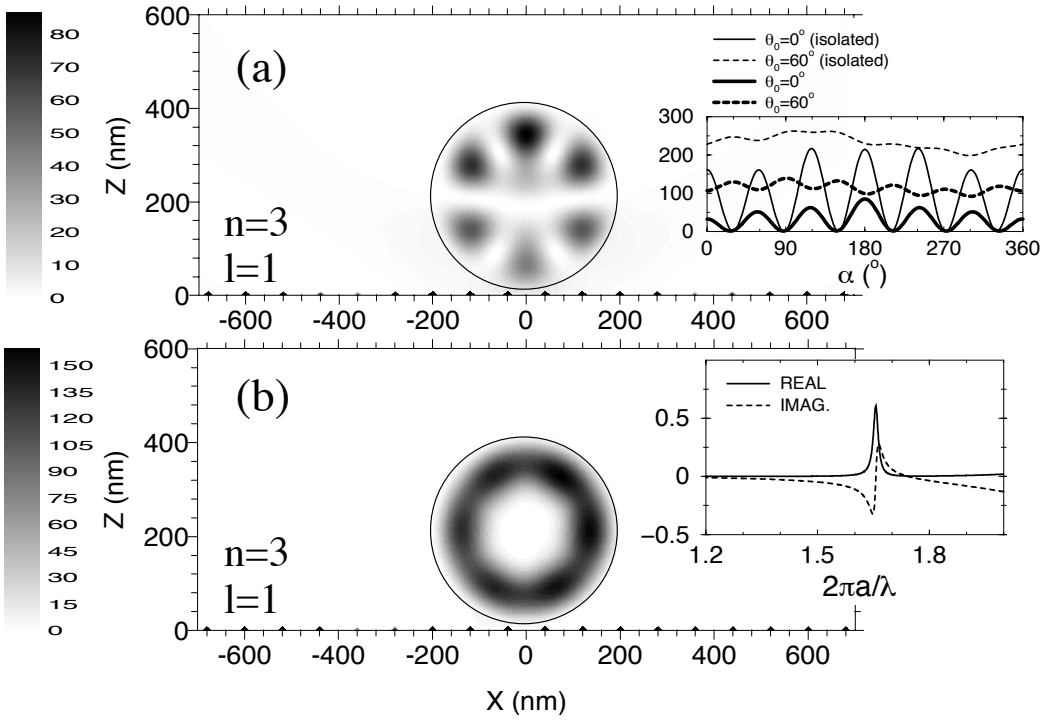

Fig. 3

J. R. Arias-Gonzalez et al.

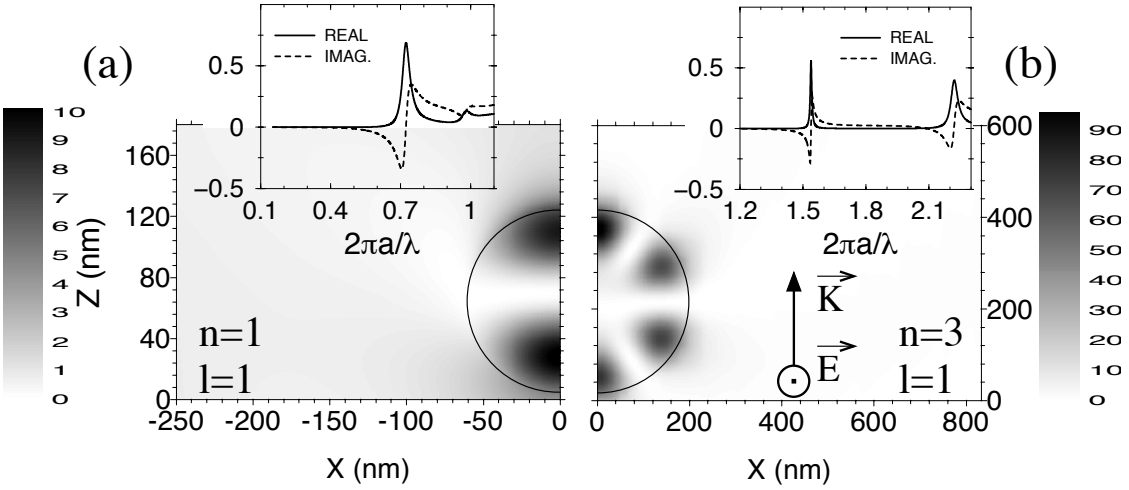

Fig. 4

J. R. Arias-Gonzalez et al.